MDPI

Article

Fabrication, Microstructure and Plasma Resistance Behavior of Y–Al–Si–O (YAS) Glass-Ceramics Coated on Alumina Ceramics

Eui Keun Park, Hwan-Yoon Jang, Seo-Yeon Jeon, Kati Raju * and Hyun-Kwuon Lee *

School of Advanced Materials Science and Engineering, Kumoh National Institute of Technology, Gumi 39177, Republic of Korea; czarkhan86@naver.com (E.K.P.); pray330@naver.com (H.-Y.J.); cilcis@naver.com (S.-Y.J.)

* Correspondence: katiraju@gmail.com (K.R.); hklee@kumoh.ac.kr (H.-K.L.); Tel.: +82-54-478-7745 (H.-K.L.); Fax: +82-54-478-7769 (H.-K.L.)

Abstract: This study investigates the fabrication, microstructural characteristics and plasma resistance of Y–Al–Si–O (YAS) glass-ceramics coated on alumina ceramics. YAS frits were initially prepared using a melt-quenching method, then homogenously milled and coated onto alumina ceramics. The melt-coating process was conducted at 1650 °C for 1 h. The composition and microstructure of the glass frits and coatings were thoroughly characterized using X-ray diffraction, scanning electron microscopy, and energy-dispersive X-ray spectroscopy. These analyses revealed a dense microstructure with a polycrystalline structure predominantly composed of $Y_3Al_5O_{12}$ (YAG) phase and a minor phase of $Y_2Si_2O_7$. The YAS coatings on alumina revealed a dense layer with strong adhesion to the substrate. Subsequently, the coatings underwent $C_4F_6/Ar/O_2$ plasma treatment for 1 h. Plasma exposure tests demonstrated that the YAS-coated alumina exhibited significantly better etching resistance compared to uncoated alumina, with minimal surface damage observed on the YAS coating, confirming its protective properties against plasma. The superior plasma resistance of YAS coatings is attributed to the predominance of its YAG phase. This research offers a more stable and cost-efficient solution for protecting ceramics in demanding plasma environments.

Keywords: alumina; microstructure; Y–Al–Si–O layer; melt coating; plasma resistance; semiconductor equipment

Citation: Park, E.K.; Jang, H.-Y.; Jeon, S.-Y.; Raju, K.; Lee, H.-K. Fabrication, Microstructure and Plasma Resistance Behavior of Y–Al–Si–O (YAS) Glass-Ceramics Coated on Alumina Ceramics. *Materials* **2024**, *17*, 4585. https://doi.org/10.3390/ma17184585

Academic Editors: Dinesh Agrawal and Csaba Balázsi

Received: 14 August 2024
Revised: 7 September 2024
Accepted: 17 September 2024
Published: 18 September 2024

Copyright: © 2024 by the authors. Licensee MDPI, Basel, Switzerland. This article is an open access article distributed under the terms and conditions of the Creative Commons Attribution (CC BY) license (https://creativecommons.org/licenses/by/4.0/).

1. Introduction

Plasma etching is a vital technique in semiconductor manufacturing, crucial for the precise patterning of integrated circuits and electronic devices. This process enables the controlled removal of material from the surface of a semiconductor wafer, achieving high-resolution features and excellent material selectivity [1–5]. These capabilities make plasma etching essential for advancing the miniaturization and performance of semiconductor devices. However, the trend towards miniaturizing electronic integrated circuits, reducing line widths and processing of high-aspect-ratio structures necessitates the use of high-power plasma. Consequently, process equipment parts must possess greater plasma resistance and high-temperature stability to withstand these demanding conditions.

Ceramics play a crucial role in plasma etching chambers, which are integral to the semiconductor manufacturing process. Various ceramic materials, such as alumina, quartz, silicon carbide and aluminum nitride, are commonly used due to their excellent thermal stability, chemical resistance and mechanical strength [6–11]. These materials are commonly employed in the form of showerheads, lift pins, insulator pipes, focus rings and confinement rings for different modules of the plasma chamber. The superior properties of ceramics ensure the durability and longevity of these etching chamber components, which are essential for maintaining the precision and efficiency of the plasma etching process. However, contamination from ceramics in plasma etching chambers presents a significant challenge [12–14]. During the etching process, ceramic materials can interact with the

reactive plasma environment, leading to the release of particulate contaminants. These contaminants can then be deposited on the semiconductor wafers, potentially causing defects and compromising the performance of the final devices.

Mitigating ceramic particle contamination in plasma etching chambers is crucial for maintaining the integrity and performance of semiconductor devices. One effective strategy is the selection and use of high-purity plasma-resistant ceramic materials for chamber components. High-purity ceramics, such as yttria, yttrium fluoride, yttrium oxyfluoride and yttrium aluminum garnet, are less prone to shedding particles under plasma exposure [15–21]. Different fluorine-based plasma gas compositions including NF_3, CF_4 and CHF_3 are investigated [12,14,17,22–25] and the results revealed that these yttrium-based ceramics exhibit improved plasma-resistance behavior when compared with alumina and quartz materials. However, high-density yttrium-based materials are cost-ineffective from a commercial standpoint.

Another vital approach involves employing protective coatings on ceramic components to create a barrier that reduces particle generation. For example, Kim et al. deposited Y_2O_3 and YF_3 coatings [17], whereas Jung et al. coated CaO-based silicate glass layers [26] on alumina ceramics and evaluated their plasma resistance behaviors. In another work, Choi et al. reported on the enhanced plasma resistance of quartz after coating with Y_2O_3-based silicate glass-ceramic through an aerosol deposition method [27]. Common methods of ceramic coating include physical vapor deposition [17], atmospheric plasma spraying [28], aerosol deposition [27,29], atomic layer deposition [30], chemical vapor deposition [31] and melt-coating [18,32]. Each method offers unique advantages, making ceramic coatings versatile solutions for enhancing durability, corrosion resistance and thermal stability. Among these, melt-coating is a versatile, cost-effective and promising technique for coating different materials. Its advantages include inexpensive equipment, rapid deposition, dense coating layer, thickness and composition control, strong adhesion to ceramics and a desirably smooth surface.

On the other hand, aluminosilicate-based glass-ceramics, including Ca–Al–Si–O, Mg–Al–Si–O, Y–Al–Si–O and RE–Al–Si–O (RE: Rare earth elements) have emerged as promising candidate materials for thermal barrier coatings, plasma etching chambers and high-temperature applications due to their exceptional properties [6,26,27,33–38]. Due to their excellent thermal stability, chemical and plasma resistance and adherence properties, Y–Al–Si–O or Y_2O_3–Al_2O_3–SiO_2 (YAS)-based glass-ceramics are particularly suited for the harsh conditions of plasma etching environments. These YAS-based coatings can effectively shield the underlying ceramic surfaces from direct exposure to reactive plasma, thereby preventing erosion and the subsequent release of contaminating particles [6,27,38]. Hence, implementing YAS-based coatings offers numerous benefits that enhance the operational efficiency and reliability of plasma etching chambers. Thus, the integration of YAS-based glass-ceramics with melt-coating technology may be considered a feasible and cost-effective approach for contamination control, supporting the stringent quality and performance standards required in modern semiconductor fabrication.

Therefore, in this study, the potential application of a typical YAS-based dense glass-ceramic coating layer on top of alumina ceramics was investigated, expecting a reduction in plasma etching behavior. Initially, YAS frits were prepared via a melt-quenching method at 1650 °C, milled homogenously and coated onto the alumina ceramics. Later, these coatings were subjected to $C_4F_6/Ar/O_2$ plasma treatment for 1 h. The objective was to evaluate the plasma resistance of alumina with YAS coatings compared to the uncoated alumina substrates, thereby demonstrating their superior plasma resistance behavior. This research provides a more stable and cost-efficient solution to protect ceramics in demanding harsh plasma environments.

2. Materials and Methods

To prepare YAS-based frits, high-purity (>99.9%) Y_2O_3, Al_2O_3 and SiO_2 powders (Kojundo, Sakado, Japan) are used in the present work. After weighing the raw material

powders according to a typical composition of 29 Y_2O_3, 33 Al_2O_3 and 38 SiO_2 (mol%), the as-received powders were thoroughly mixed. This composition was chosen in view of its excellent $Y_3Al_5O_{12}$ (YAG) and $Y_2Si_2O_7$ phase-forming ability, which is located at the eutectic point of the Y_2O_3–Al_2O_3–SiO_2 phase diagram [39,40]. To ensure a homogeneous distribution of phases in the mixture, ball milling was performed with alumina balls for 4 h using ethanol as the dispersion medium. The mixed slurry was vacuum-dried at 110 °C for 24 h. Later, the obtained powder mixture was placed in a platinum crucible, heat treated at 1650 °C for 2 h in a furnace, and then cooled to obtain YAS-based frits. As-prepared YAS frits were ground thoroughly using planetary ball milling (Pulverisette 6, Fritsch, Idar-Oberstein, Germany), applied in the form of a slurry to the surface of the Al_2O_3 base materials and then melt-coated at 1650 °C for 1 h. More details about the processing can be found in the literature [26]. Disc-shaped (12 mm diameter and 4 mm thickness) alumina ceramics with a relative density of 99% or higher manufactured using commercial Al_2O_3 powder (AL-160SG, Showa Denko, Oyama City, Japan) were used as the base materials in this study. Sintering of alumina ceramics was performed in air using a furnace at 1650 °C for 2 h. All the specimens were polished thoroughly before coating in order to obtain a smooth and homogenous deposition.

The particle sizes of raw powders were investigated using a laser-diffraction particle size analyzer (PSA, Mastersizer 2000, Malvern, UK). The microstructures of the prepared frit and coating layer specimens were observed using a field emission scanning electron microscope (FE-SEM, JEOL, Tokyo, Japan) and the composition analysis of each crystal phase was performed using an Energy Dispersive X-ray spectrometer (EDS) attached to the FE-SEM. An X-ray diffractometer (XRD, Rigaku, Tokyo, Japan) with Cu Kα radiation (λ = 0.15406 nm) was used to analyze the phase structures of the frit and coating layer at room temperature. The frit was powdered and the coating layer was polished smoothly before measurement. Phase fractions were calculated using the integrated intensities of all crystalline and amorphous phases of the measured XRD patterns. Plasma etching tests were performed on specimens with and without YAS coating for 1 h with C_4F_6, Ar and O_2 gasses using TCP-9600PTX (LAM Research Co., Fremont, CA, USA) equipment. The detailed experimental conditions are presented in Table 1. For this purpose, half of the specimens' surfaces were masked with polyimide tape (Figure S1). The etching rate was evaluated through the weight reduction rate per unit area of the specimens before and after plasma etching. An electronic micro balance with a readability of 10^{-4} g was used to measure the weight of the specimens. The surfaces of all the specimens were polished using diamond paste before plasma treatment.

Table 1. Plasma etching conditions used in the present work.

Parameter	Condition
Top RF power (W)	900
Bottom RF power (W)	200
C_4F_6 (Sccm)	30
Ar (Sccm)	60
O_2 (Sccm)	15
Pressure (mTorr)	10
Operating time (h)	1

3. Results and Discussion

Figure 1 presents SEM micrographs of the as-received raw powders Y_2O_3, Al_2O_3 and SiO_2. These images demonstrate that all the raw powders contain fine and micron-sized particles with irregular morphologies. PSA analysis (Figure S2) revealed average particle sizes of about 4.4, 2.7 and 0.7 μm, respectively, for Y_2O_3, Al_2O_3 and SiO_2 raw powders. These findings are consistent with the observations from the SEM images.

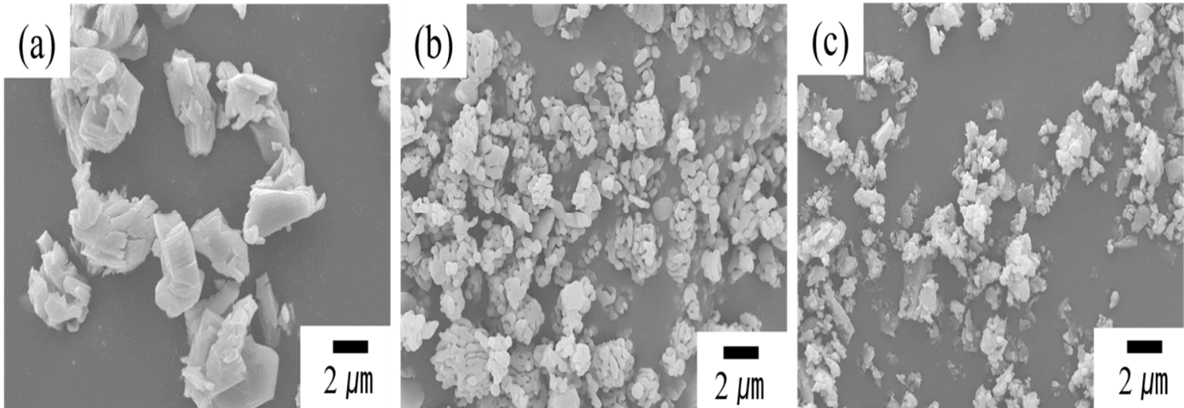

Figure 1. SEM micrographs of the as-received raw powders (**a**) Y_2O_3, (**b**) Al_2O_3 and (**c**) SiO_2. These images demonstrate that all the raw powders contain fine and micron-sized particles with irregular morphologies.

Figure 2a shows the XRD patterns of YAS frit after heat treatment at 1650 °C. The controlled heat treatment resulted in the formation of glass-ceramics, as indicated by the XRD analysis, which revealed a polycrystalline structure predominantly composed of a major phase of YAG (JCPDS card no:79–1891) [41] and a minor phase of $Y_2Si_2O_7$ (JCPDS card no:42–0168) [41]. This suggests that, at this temperature, the glass powders underwent sufficient crystallization to form YAG and $Y_2Si_2O_7$ phases, followed by sintering to produce dense and bulk glass-ceramics. According to the literature, $Y_2Si_2O_7$ exhibits rich polymorphism and transforms into the δ-phase at high temperatures [41,42]. The crystalline phases detected in this study are generally consistent with those expected from the equilibrium phase diagram. YAS glass-ceramics can precipitate a variety of crystalline phases such as YAG, $Al_6Si_2O_{13}$, $Y_4Al_2O_9$, Y_2SiO_5 and $Y_2Si_2O_7$, depending on the initial composition, as indicated by the phase diagram [39,40,43–46]. Among these, YAS glass-ceramics with YAG as the main crystalline phase are preferred due to their excellent plasma-corrosion resistance properties [20].

The phase fractions (%) were calculated using the intensity ratio method, based on the sum of the integrated intensities of all crystalline and amorphous phases present in the measured XRD patterns [47,48]. The analysis revealed 69.66% YAG phase, 27.36% $Y_2Si_2O_7$ phase and 2.98% YAS amorphous (glass) phase.

Figure 2b shows an SEM (BSE mode) image of a typical YAS frit, revealing a dense microstructure. This figure shows mainly light gray grains with two different morphologies, both large and small. EDS elemental distribution analysis, shown in Figure 2c, revealed the presence of Y, Al, Si and O elements only. Based on the EDS point analysis (Figure S3), the large grains were identified as the YAG phase, while the small grains were identified as the $Y_2Si_2O_7$ phase. EDS analysis indicated that the YAG phase consists of 16.37 %, 24.90 % and 58.73 % of Y, Al and O elements (at. %), respectively. In contrast, the $Y_2Si_2O_7$ phase contains 19.28 %, 18.24 % and 62.48 % of Y, Si and O elements (at. %), respectively. The dark gray phase was identified as the YAS amorphous (glass) phase. These findings are consistent with the XRD data shown in Figure 2a.

BSE–SEM and EDS were used to examine the microstructure and elemental distribution of the YAS layer after coating on alumina, and the results are displayed in Figure 3. The BSE–SEM image of a typical YAS coating layer is presented in Figure 3a and the corresponding EDS mapping image is displayed in Figure 3b. No pores were found in the deposited coatings (Figure 3a), indicating a dense microstructure. The image shows grains with two distinct contrasts and morphologies: dark gray and light gray, with varying sizes. According to the EDS mapping results, the light gray region with larger grain sizes is rich in Y, Al and O elements, while the light gray region with smaller grain sizes is rich in Y, Si and O elements. Based on these EDS mapping data combined with XRD patterns, it was

concluded that the gray phase with larger grain size corresponds to the YAG phase, the light gray phase with smaller grain size corresponds to the $Y_2Si_2O_7$ phase and the minor dark gray phase corresponds to the amorphous (glass) YAS phase. The microstructure is similar to that of glass frit (Figure 2b), and its XRD analysis (Figure S4) also revealed major peaks of YAG phase and minor peaks of $Y_2Si_2O_7$ phase. The phase fractions (%) were calculated to be 77.64% YAG phase, 13.68% $Y_2Si_2O_7$ phase and 8.68% YAS amorphous (glass) phase. These phase categories and their distribution did not differ much from those of the glass frit before coating, and these results are in consistent with previous findings [41,44]. Minor variations in the phase fractions compared to the glass frit may be attributed to the altered mol% of Al_2O_3 content from the alumina substrate. From the above microstructural analyses, it has been confirmed that the two crystalline phases present in the YAS system are YAG and $Y_2Si_2O_7$.

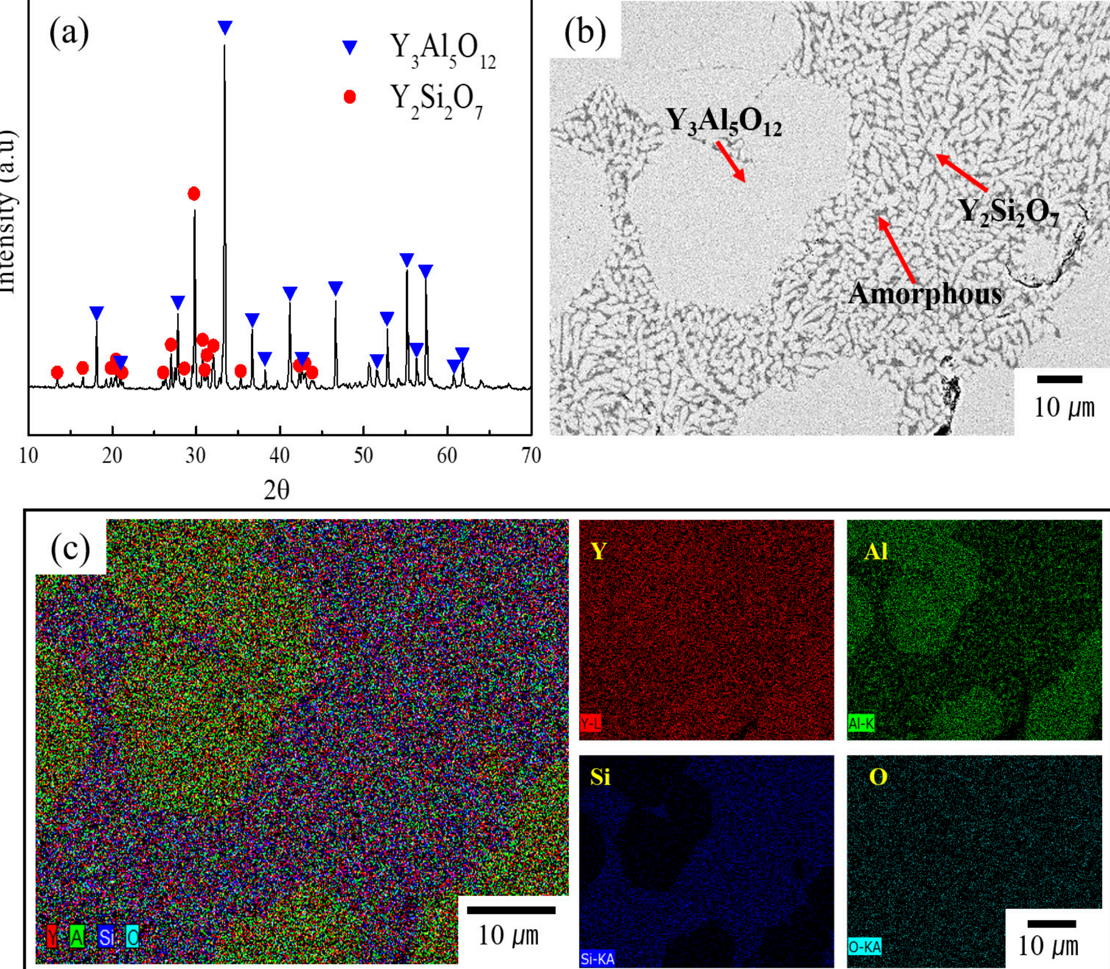

Figure 2. (**a**) XRD patterns of YAS frit after heat treatment at 1650 °C. The controlled heat treatment resulted in the formation of glass-ceramics, which revealed a polycrystalline structure predominantly composed of a major phase of YAG (JCPDS card no:79–1891) [41] and minor phase of $Y_2Si_2O_7$ (JCPDS card no:42–0168) [41]. (**b**) SEM (BSE mode) image of typical YAS frit, revealing a dense microstructure. (**c**) EDS elemental mapping and elemental distribution of Y, Al, Si and O elements. This figure shows mainly light gray grains with two different morphologies, both large and small. Based on the EDS point analysis, the large grains were identified as the YAG phase and small grains as the $Y_2Si_2O_7$ phase. The dark gray phase was identified as the YAS amorphous (glass) phase.

Figure 4 shows a BSE–cross-sectional micrograph of YAS-coated alumina, which reveals a dense microstructure. The coating–substrate interface cross-sectional SEM image with the corresponding EDS elemental mapping is shown in Figure S5 and reveals that the coating layer

has a thickness of 110 μm. Strong adhesion between the coating layer and the pristine alumina, without cracks, can be seen at the interface. XRD, SEM and EDS analyses revealed major peaks corresponding to the YAG phase and minor peaks corresponding to the $Y_2Si_2O_7$ phase. These phase categories are identical to those observed in the YAS glass frit and coating layers.

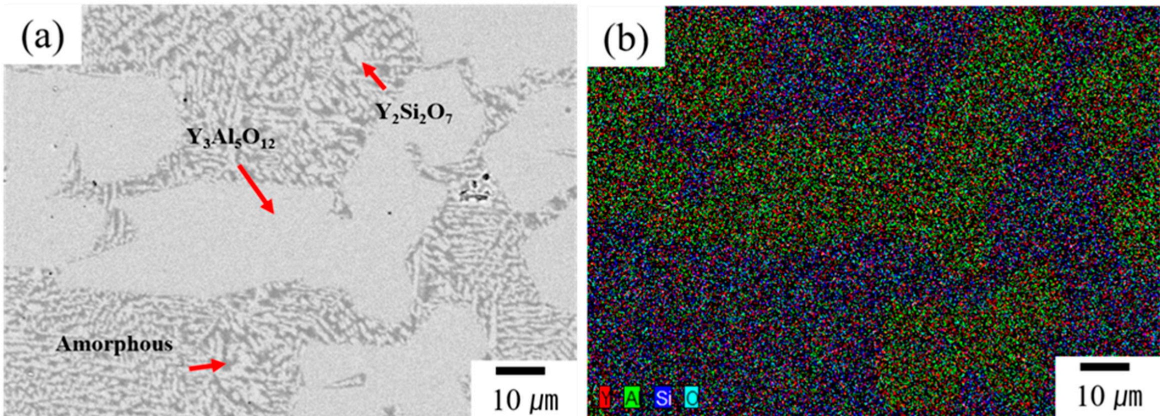

Figure 3. (**a**) BSE−SEM image of a typical YAS coating layer and (**b**) its corresponding EDS mapping image. No pores were found in the deposited coatings, indicating a dense microstructure. The image shows grains with two distinct contrasts and morphologies: dark gray and light gray, with varying sizes. According to the EDS mapping results, the light gray region with larger grain sizes is rich in Y, Al and O elements, while the light gray region with smaller grain sizes is rich in Y, Si and O elements.

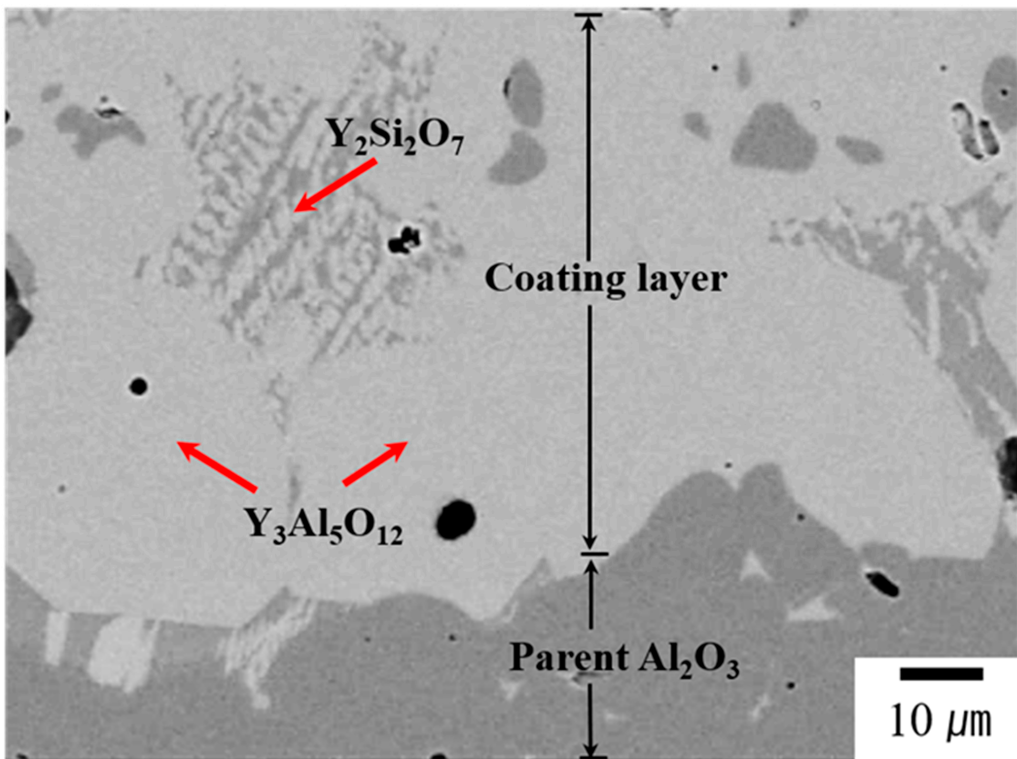

Figure 4. BSE–cross-sectional micrograph of YAS-coated alumina and it reveals a dense microstructure. Strong adhesion between the coating layer and the pristine alumina, without cracks, can be seen at the interface. Analyses revealed major peaks corresponding to YAG phase and minor peaks corresponding to $Y_2Si_2O_7$ phase. These phase categories are identical to those observed in the YAS glass frit and coating layers.

The surface morphology of the specimens was examined using SEM to assess damage after plasma exposure. Figure 5 presents the SEM images of the surface microstructures of uncoated (pristine) and YAS-coated alumina ceramics post-exposure to plasma. Figure 5a,b compares both etched and non-etched regions. No noticeable difference in the surface microstructure of YAS coatings was observed before and after plasma exposure when compared to pristine alumina. High-magnification-surface SEM images after plasma treatment for uncoated and coated specimens are compared in Figure 5c,d, respectively. Many crater-like erosion sites were observed on the surface of the alumina (Figure 5c) following plasma exposure, whereas minimal surface damage was observed on the YAS-coated layer (Figure 5d). The high-Y region showed less plasma-induced erosion compared to the low-Y region. The surface morphological changes illustrated in this figure support this observation. According to the SEM images in Figure 5, the surface erosion of alumina was significant, while the YAS-coated layer demonstrated good etching resistance to plasma. It was observed that the surface of YAG phase appeared undamaged, but the material loss was relatively higher in the $Y_2Si_2O_7$ phase.

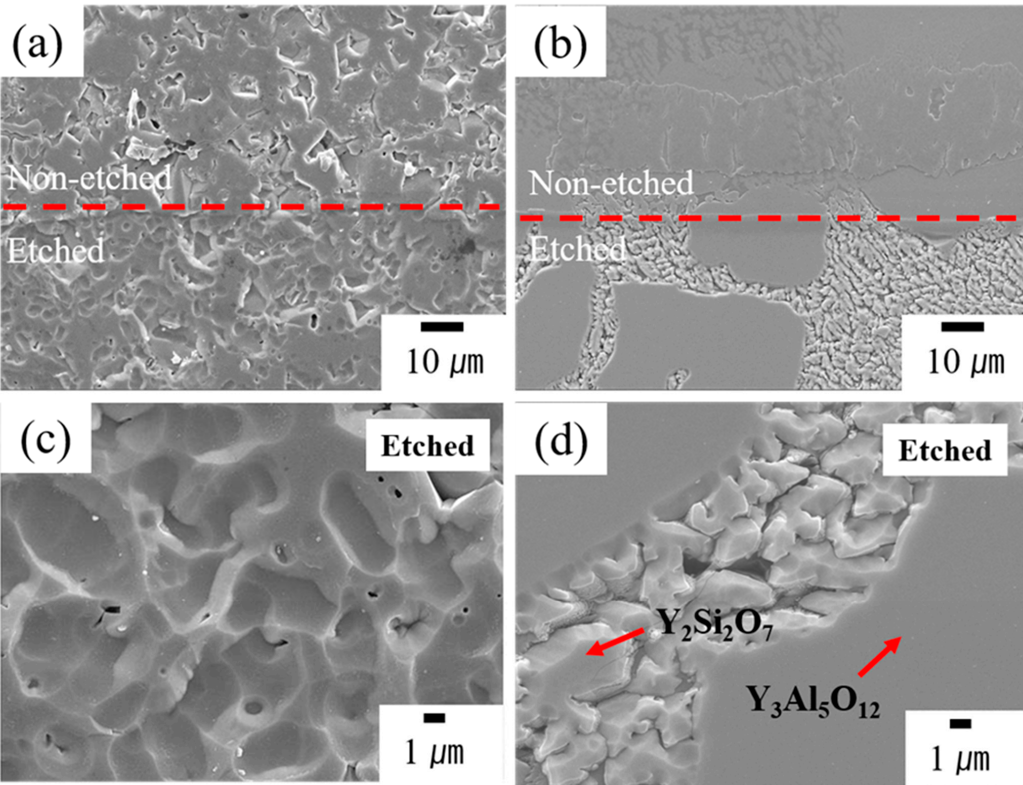

Figure 5. SEM images of the surface microstructures of both etched and non-etched regions of (**a**) uncoated (pristine) and (**b**) YAS-coated alumina ceramics post-exposure to plasma. No noticeable difference in the surface microstructure of YAS coatings was observed before and after exposure plasma exposure, compared to pristine alumina. High magnification surface SEM images after plasma treatment for (**c**) uncoated and (**d**) YAS-coated specimens.

Pristine alumina exhibited a noticeable etching loss of 0.0148% per square centimeter, whereas the YAS-coated layer showed a minimal loss of 0.0047% per square centimeter (about three times enhancement). The improved plasma-etching behavior of the YAS coating is likely due to the predominance of the YAG phase. It has been reported that materials containing Si react with F radicals in the plasma to form compounds with low sublimation points, which volatilize quickly. In contrast, the YAG phase reacts with F radicals to form fluorine compounds with very high sublimation points, resulting in a low etching rate [6]. Previous studies have shown that the YAG phase exhibits good resistance to fluorocarbon plasma corrosion, partly due to the rare-earth elements it contains, which

inhibit reactions with fluorine-containing plasmas [20,49,50]. Additionally, the fluorides generated do not volatilize easily and form a protective layer on the ceramic surface, preventing further corrosion. Further investigations are required to analyze plasma etching behavior in more detail, particularly for the $Y_2Si_2O_7$ phase.

4. Conclusions

In conclusion, the results indicate that YAS glass-ceramics, particularly with YAG as the predominant phase, exhibit excellent plasma-corrosion resistance. SEM and XRD analyses confirm the formation of YAG and $Y_2Si_2O_7$ phases in the glass-ceramics, with microstructural analysis showing a dense, well-adhered coating on the alumina. Plasma exposure tests reveal that the YAS-coated alumina demonstrates minimal surface damage compared to uncoated alumina, highlighting the effectiveness of YAG in enhancing plasma resistance. These findings suggest that YAS coatings are highly effective for applications requiring resistance to plasma-induced corrosion. Further research is recommended to explore the detailed plasma etching behavior and optimize coating formulations for improved performance.

Supplementary Materials: The following supporting information can be downloaded at: https://www.mdpi.com/article/10.3390/ma17184585/s1, Figure S1: Specimen's configuration used for plasma exposure tests. Half of the specimen's surface was masked with polyimide tape; Figure S2: PSA analysis of Y_2O_3, Al_2O_3 and SiO_2 raw powders and it revealed average particle sizes of about 4.4, 2.7 and 0.7 μm, respectively; Figure S3: BSE SEM image and EDS analysis points of YAS frit. The large grains were identified as the YAG phase, while the small grains were identified as the $Y_2Si_2O_7$ phase. EDS analysis indicated that the YAG phase consists (Point A) of 16.37%, 24.90%, and 58.73% of Y, Al and O elements (at. %), respectively. In contrast, the $Y_2Si_2O_7$ (Point B) contains 19.28%, 18.24%, and 62.48% of Y, Si and O elements (at. %), respectively. The dark gray phase was identified as the YAS amorphous (glass) phase; Figure S4: XRD patterns of YAS-coated layer. The analysis revealed major peaks of YAG phase and minor peaks of $Y_2Si_2O_7$ phase. The phase fractions (%) were calculated to be 77.64% YAG phase, 13.68% $Y_2Si_2O_7$ phase, and 8.68% YAS amorphous (glass) phase; Figure S5: BSE−cross-sectional micrograph of YAS-coated alumina and its elemental mapping.

Author Contributions: Conceptualization, E.K.P. and H.-K.L.; Data curation, E.K.P., H.-Y.J. and S.-Y.J.; Formal analysis, E.K.P., H.-Y.J., S.-Y.J. and K.R.; Funding acquisition, H.-K.L.; Methodology, E.K.P., K.R. and H.-K.L.; Resources, H.-K.L.; Supervision, H.-K.L.; Writing—original draft, E.K.P. and K.R.; Writing—review and editing, K.R. and H.-K.L. All authors have read and agreed to the published version of the manuscript.

Funding: This research was supported by the Kumoh national Institute of Technology (2022~2023).

Institutional Review Board Statement: Not applicable.

Informed Consent Statement: Not applicable.

Data Availability Statement: The original contributions presented in the study are included in the article/Supplementary Material, further inquiries can be directed to the corresponding authors.

Conflicts of Interest: The authors declare no conflicts of interest.

References

1. Abe, H.; Yoneda, M.; Fujiwara, N. Developments of Plasma Etching Technology for Fabricating Semiconductor Devices. *Jpn. J. Appl. Phys.* **2008**, *47*, 1435–1455. [CrossRef]
2. Banna, S.; Agarwal, A.; Cunge, G.; Darnon, M.; Pargon, E.; Joubert, O. Pulsed High-density Plasmas for Advanced Dry Etching Processes. *J. Vac. Sci. Technol. A* **2012**, *30*, 040801. [CrossRef]
3. Economou, D.J. Pulsed Plasma Etching for Semiconductor Manufacturing. *J. Phys. D Appl. Phys.* **2014**, *47*, 303001. [CrossRef]
4. Chun, I.; Efremov, A.; Yeom, G.Y.; Kwon, K.-H. A comparative study of $CF_4/O_2/Ar$ and $C_4F_8/O_2/Ar$ Plasmas for Dry Etching Applications. *Thin Solid Film.* **2015**, *579*, 136–143. [CrossRef]
5. Oehrlein, G.S.; Brandstadter, S.M.; Bruce, R.L.; Chang, J.P.; DeMott, J.C.; Donnelly, V.M.; Dussart, R.; Fischer, A.; Gottscho, R.A.; Hamaguchi, S.; et al. Future of Plasma Etching for Microelectronics: Challenges and Opportunities. *J. Vac. Sci. Technol. B* **2024**, *42*, 041501. [CrossRef]

6. Choi, J.H.; Im, W.B.; Kim, H.-J. Plasma Resistant Glass (PRG) for Reducing Particulate Contamination During Plasma Etching in Semiconductor Manufacturing: A Review. *Mater. Today Commun.* **2023**, *34*, 105267. [CrossRef]
7. Kim, D.-M.; Kim, K.-B.; Yoon, S.-Y.; Oh, Y.-S.; Kim, H.-T.; Lee, S.-M. Effect of Artificial Pores and Purity on the Erosion Behaviors of Polycrystalline Al_2O_3 Ceramics under Fluorine Plasma. *J. Ceram. Soc. Jpn.* **2009**, *117*, 863–867. [CrossRef]
8. Kasashima, Y.; Tabaru, T.; Matsuda, O.; Motomura, T. Investigation of the Relationship between Plasma Etching Characteristics and Microstructures of Alumina Ceramics for Chamber Parts. *Jpn. J. Appl. Phys.* **2019**, *58*, 041001. [CrossRef]
9. Jang, M.-R.; Paek, Y.-K.; Lee, S.-M. Plasma Resistance and Etch Mechanism of High Purity SiC under Fluorocarbon Plasma. *J. Korean Ceram. Soc.* **2012**, *49*, 328–332. [CrossRef]
10. Garcia-Rosales, C. Erosion Processes in Plasma-wall Interactions. *J. Nucl. Mater.* **1994**, *211*, 202–214. [CrossRef]
11. Wang, X.; Lee, H.; Nam, S.K.; Kushner, M.J. Erosion of Focus Rings in Capacitively Coupled Plasma Etching Reactors. *J. Vac. Sci. Technol. A* **2021**, *39*, 063002. [CrossRef]
12. Song, J.B.; Kim, J.T.; Oh, S.G.; Yun, J.Y. Contamination Particles and Plasma Etching Behavior of Atmospheric Plasma Sprayed Y_2O_3 and YF_3 Coatings under NF_3 Plasma. *Coatings* **2019**, *9*, 102. [CrossRef]
13. Ito, N.; Moriya, T.; Uesugi, F.; Matsumoto, M.; Liu, S.; Kitayama, Y. Reduction of Particle Contamination in Plasma-etching Equipment by Dehydration of Chamber Wall. *Jpn. J. Appl. Phys.* **2008**, *47*, 3630–3634. [CrossRef]
14. So, J.; Kim, M.; Kwon, H.; Maeng, S.; Choi, E.; Chung, C.-W.; Yun, J.-Y. Investigation of Contamination Particles Generation and Surface Chemical Reactions on Al_2O_3, Y_2O_3, and YF_3 Coatings in F-based Plasma. *Appl. Surf. Sci.* **2023**, *629*, 157367. [CrossRef]
15. Kim, C.S.; Kim, M.J.; Cho, H.; Park, T.-E.; Yun, Y.-H. Fabrication and Plasma Resistance of Y_2O_3 Ceramics. *Ceram. Int.* **2015**, *41*, 12757–12762. [CrossRef]
16. Ashizawa, H.; Yoshida, K. Effect of the Microstructures of Yttria Ceramics on Their Plasma Corrosion Behavior. *Ceram. Int.* **2019**, *45*, 21162–21167. [CrossRef]
17. Kim, D.-M.; Oh, Y.-S.; Kim, S.; Kim, H.-T.; Lim, D.-S.; Lee, S.-M. The Erosion Behaviors of Y_2O_3 and YF_3 Coatings under Fluorocarbon Plasma. *Thin Solid Film.* **2011**, *519*, 6698–6702. [CrossRef]
18. Shiba, Y.; Teramoto, A.; Goto, T.; Kishi, Y.; Shirai, Y.; Sugawa, S. Stable Yttrium Oxyfluoride Used in Plasma Process Chamber. *J. Vac. Sci. Technol. A* **2017**, *35*, 021405. [CrossRef]
19. Miyashita, K.; Tsunoura, T.; Yoshida, K.; Yano, T.; Kishi, Y. Fluorine and Oxygen Plasma Exposure Behavior of Yttrium Oxyfluoride Ceramics. *Jpn. J. Appl. Phys.* **2019**, *58*, SEEC01. [CrossRef]
20. Qin, X.; Zhou, G.; Yang, H.; Wong, J.I.; Zhang, J.; Luo, D.; Wang, S.; Ma, J.; Tang, D. Fabrication and Plasma Resistance Properties of Transparent YAG ceramics. *Ceram. Int.* **2012**, *38*, 2529–2535. [CrossRef]
21. Cao, Y.-C.; Zhao, L.; Luo, J.; Wang, K.; Zhang, B.-P.; Yokota, H.; Ito, Y.; Li, J.-F. Plasma Etching Behavior of Y_2O_3 Ceramics: Comparative Study with Al_2O_3. *Appl. Surf. Sci.* **2016**, *366*, 304–309. [CrossRef]
22. Park, S.H.; Kim, K.E.; Hong, S.J. Surface Analysis of Chamber Coating Materials Exposed to CF_4/O_2 Plasma. *Coatings* **2021**, *11*, 105. [CrossRef]
23. Lee, S.; Lee, J.; Kim, W.; Hwang, N.-M. Plasma Etching Behavior of YOF Coating Deposited by Suspension Plasma Spraying in Inductively Coupled CHF_3/Ar Plasma. *Coatings* **2020**, *10*, 1023. [CrossRef]
24. Lin, T.-K.; Wang, W.-K.; Huang, S.-Y.; Tasi, C.-T.; Wuu, D.-S. Comparison of Erosion Behavior and Particle Contamination in Mass-Production CF_4/O_2 Plasma Chambers Using Y_2O_3 and YF_3 Protective Coatings. *Nanomaterials* **2017**, *7*, 183. [CrossRef] [PubMed]
25. Lee, Y.; Yeom, H.; Choi, D.; Kim, S.; Lee, J.; Kim, J.; Lee, H.; You, S. Database Development of SiO_2 Etching with Fluorocarbon Plasmas Diluted with Various Noble Gases of Ar, Kr, and Xe. *Nanomaterials* **2022**, *12*, 3828. [CrossRef] [PubMed]
26. Jung, Y.S.; Min, K.W.; Choi, J.H.; Yoon, J.S.; Im, W.B.; Kim, H.-J. Plasma-resistant Characteristics According to Sintering Conditions of CaO–Al_2O_3–SiO_2 Glass Coating layer. *J. Korean Ceram. Soc.* **2022**, *59*, 86–93. [CrossRef]
27. Choi, S.; Jeong, D.-Y.; Kim, H. Plasma Resistance of Quartz with a Glass Coating Layer by Aerosol Deposition. *Adv. Appl. Ceram.* **2018**, *117*, 328–333. [CrossRef]
28. Kreethi, R.; Hwang, Y.-J.; Lee, H.-Y.; Park, J.-H.; Lee, K.-A. Stability and Plasma Etching Behavior of Yttrium-based Coatings by Air Plasma Spray Process. *Surf. Coat. Technol.* **2023**, *454*, 129182. [CrossRef]
29. Iwasawa, J.; Nishimizu, R.; Tokita, M.; Kiyohara, M.; Uematsu, K. Plasma-resistant Dense Yttrium Oxide Film Prepared by Aerosol Deposition Process. *J. Am. Ceram. Soc.* **2007**, *90*, 2327–2332. [CrossRef]
30. Niinisto, J.; Putkonen, M.; Niinisto, L. Processing of Y_2O_3 Thin Films by Atomic Layer Deposition from Cyclopentadienyl-type Compounds and Water as Precursors. *Chem. Mater.* **2004**, *16*, 2953–2958. [CrossRef]
31. Banal, R.; Kimura, T.; Goto, T. High Speed Deposition of Y_2O_3 Films by Laser Assisted Chemical Vapor Deposition. *Mater. Trans.* **2005**, *46*, 2114–2116. [CrossRef]
32. Park, E.K.; Lee, H.-K. Fabrication of Plasma Resistant Y_2O_3-Al_2O_3-SiO_2 Coating Ceramics by Melt-Coating Method. *Korean J. Mater. Res.* **2020**, *30*, 359–368. [CrossRef]
33. Mlainverni, C.; Salvo, M.; Zietara, M.; Cempura, G.; Kruk, A.; Maier, J.; Prentice, C.; Farnham, M.; Casalengo, V. A Yttrium Aluminosilicate Glass-Ceramic to Join SiC/SiC Composites. *J. Eur. Ceram. Soc.* **2024**, *44*, 3579–3587. [CrossRef]
34. Park, J.; Choi, J.H.; Na, H.; Kim, H.J. Effect of CaF_2 on Fluorocarbon Plasma Resistance and Thermal Properties of CaO-Al_2O_3-SiO_2 Glasses. *J. Asian Ceram. Soc.* **2021**, *9*, 311–317. [CrossRef]

35. Gao, C.; Zhao, X.; Li, B. Influence of Y_2O_3 on Microstructure, Crystallization, and Properties of MgO-Al_2O_3-SiO_2 Glass-Ceramics. *J. Non-Cryst. Solids* **2021**, *560*, 120728. [CrossRef]
36. Na, H.; Park, J.; Choi, S.C.; Kim, H.J. The Effect of Composition of Plasma Resistance of CaO–Al_2O_3–SiO_2 Glasses under Fluorocarbon Plasma with Ar^+. *Appl. Surf. Sci.* **2019**, *476*, 663–667. [CrossRef]
37. Ma, Y.; Guo, C.; Cui, Y.; Yang, S.; Meng, X.; Kou, S.; Luan, C.; Deng, J.; Fan, S. Enhanced Water-Oxygen Corrosion Resistance of SiC/SiC Composites at 1350 °C via Single-Layer Y-Al-Si-O Glass-Ceramics Environmental Barrier Coatings. *J. Eur. Ceram. Soc.* **2024**, *44*, 116728. [CrossRef]
38. Lee, J.; Kim, D.; Lee, S.; Kim, H. Effect of Rare-earth Elements on the Plasma Etching Behavior of the RE-Si-Al-O Glasses. *J. Non-Cryst. Solids* **2012**, *358*, 898–902. [CrossRef]
39. Fabrichnaya, O.; Seifert, H.J.; Weiland, R.; Ludwig, T.; Aldinger, F.; Navrotsky, A. Phase Equilibria and Thermodynamics in the Y_2O_3–Al_2O_3–SiO_2 System. *Int. J. Mater. Res.* **2001**, *92*, 1083–1097.
40. Bondar, I.A.; Galakhov, F.Y. Phase Equilibria in the System Y_2O_3-Al_2O_3-SiO_2. *Russ. Chem. Bull.* **1964**, *13*, 1231–1232. [CrossRef]
41. Sadiki, N.; Coutures, J.P.; Fillet, C.; Dussossoy, J.L. Crystallization of Lanthanum and Yttrium Aluminosilicate Glasses. *J. Nucl. Mater.* **2006**, *348*, 70–78. [CrossRef]
42. Parmentier, J.; Bodart, P.R.; Audoin, L.; Massouras, G.; Thompson, D.P.; Harris, R.K.; Goursat, P.; Besson, J.-L. Phase Transformations in Gel-Derived and Mixed-Powder-Derived Yttrium Disilicate, $Y_2Si_2O_7$, by X-Ray Diffraction and ^{29}Si MAS NMR. *J. Solid State Chem.* **2000**, *149*, 16–20. [CrossRef]
43. Kolitsch, U.; Seifert, H.J.; Ludwig, T.; Aldinger, F. Phase Equilibria and Crystal Chemistry in the Y_2O_3–Al_2O_3–SiO_2 System. *J. Mater. Res.* **1999**, *14*, 447–455. [CrossRef]
44. Ahmad, S.; Ludwig, T.; Herrmann, M.; Mahmoud, M.M.; Lippmann, W.; Seifert, H.J. Phase Evaluation During High Temperature Long Heat Treatments in the Y_2O_3–Al_2O_3–SiO_2 system. *J. Eur. Ceram. Soc.* **2014**, *34*, 3835–3840. [CrossRef]
45. Kolitsch, U.; Scifert, H.J.; Aldinger, F. Phase Relationships in the Systems RE_2O_3-Al_2O_3-SiO_2 (RE = rare earth element, Y, and Sc). *J. Phase Equilibria* **1998**, *19*, 426–433. [CrossRef]
46. Zhang, Y.; Navrotsky, A. Thermochemistry of Glasses in the Y_2O_3-Al_2O_3-SiO_2 System. *J. Am. Ceram. Soc.* **2003**, *86*, 1727–1732. [CrossRef]
47. Shah, B.; Kakumanu, V.K.; Bansal, A.L. Analytical Techniques for Quantification of Amorphous/Crystalline Phases in Pharmaceutical Solids. *J. Pharm. Sci.* **2006**, *95*, 1641–1665. [CrossRef]
48. Anantharaman, S.B.; Rajkumar, V.B.; Raghunandan, S.; Kumer, K.C.H.; Kumar, R.S. Role of Thermodynamic Miscibility Gaps in Phase Selection in Sol-gel Synthesis of Yttrium Silicates. *J. Eur. Ceram. Soc.* **2017**, *37*, 5001–5007. [CrossRef]
49. Zhao, C.-C.; Kim, E.-B.; Park, Y.-J.; Logesh, G.; Kim, M.-J.; Lee, J.-W.; Ma, H.J.; Kim, H.-N.; Ko, J.-W.; Yoon, S.-Y. Optimization of a TEOS addition on plasma resistance of YAG ceramics. *Int. J. Appl. Ceram. Technol.* **2024**, *21*, 3200–3208. [CrossRef]
50. Zhao, C.-C.; Kim, E.-B.; Park, Y.-J.; Logesh, G.; Kim, M.-J.; Lee, J.-W.; Ma, H.J.; Kim, H.-N.; Ko, J.-W.; Yoon, S.-Y. Optimization of Al-excess nonstoichiometry on the densification and plasma resistance of YAG ceramics. *Ceram. Int.* **2024**, *50*, 15325–15332. [CrossRef]

Disclaimer/Publisher's Note: The statements, opinions and data contained in all publications are solely those of the individual author(s) and contributor(s) and not of MDPI and/or the editor(s). MDPI and/or the editor(s) disclaim responsibility for any injury to people or property resulting from any ideas, methods, instructions or products referred to in the content.